Progress In Electromagnetics Research B, Vol. 63, 173–186, 2015

Scattering of an Obliquely Incident Plane Electromagnetic Wave by a Magnetized Plasma Column: Energy Flow Patterns at Plasmon Resonances

Vasiliy A. Es'kin, Alexander V. Ivoninsky, and Alexander V. Kudrin*

Abstract—The scattering of an obliquely incident H-polarized plane electromagnetic wave by a magnetized plasma column is studied. It is assumed that the column is located in free space and aligned with an external static magnetic field. The emphasis is placed on the case where the angular frequency of the incident wave coincides with one of the surface- or volume-plasmon resonance frequencies of the column. The spatial structures of the field and energy flow patterns in the near zone of the column are analyzed, and the location of the regions with a greatly enhanced magnitude of the time-averaged Poynting vector is determined. It is shown that the sign reversal of the longitudinal energy-flow component that is parallel to the column axis can occur when passing across the boundary between the inner region of the column and the surrounding medium.

1. INTRODUCTION

The problem of scattering of plane electromagnetic waves by various cylindrical objects has been studied for a long time (see, e.g., [1] and references therein). Of special interest is the case where the scatterers possess gyrotropic properties. In the optical range, this interest is stimulated by promising applications of systems with nanosized gyrotropic elements [2], photonic crystals on the basis of gyrotropic scatterers [3], and nonreciprocal devices containing magnetooptic materials [4, 5]. In the RF range, the corresponding analysis is needed for consideration of the excitation and propagation of electromagnetic waves in the presence of artificial plasma density irregularities aligned with an external static magnetic field [6], especially if the excitation source is located outside such a plasma structure, rather than inside of it [7] or on its surface [8]. Since the understanding of the features of wave diffraction by gyrotropic cylindrical structures often requires knowledge of the field distribution near scatterers, the problem of finding the near-zone scattered fields turns out to be very topical. For many applications, the structure of the energy flow pattern in proximity to a cylindrical gyrotropic scatterer can be of primary importance. However, this problem was considered in some detail only in the special case of normal incidence of an H wave on the gyrotropic cylinder [9]. It is the purpose of this work to extend the analysis of [9] to the case of oblique incidence of a plane electromagnetic wave on the gyrotropic cylindrical scatterer.

Since the full analysis of the above-formulated problem would take up much space, in this work we restrict ourselves to consideration of the case where an H-polarized plane electromagnetic wave is obliquely incident on a magnetized plasma column aligned with an external static magnetic field. We focus our attention on the spatial structures of the electromagnetic field and the time-averaged energy flow patterns during the resonance scattering when the frequency of the incident radiation

Received 4 August 2015, Accepted 11 September 2015, Scheduled 18 September 2015

* Corresponding author: Alexander V. Kudrin (kud@rf.unn.ru).
The authors are with the Department of Radiophysics, University of Nizhny Novgorod, 23 Gagarin Avenue, Nizhny Novgorod 603950, Russia.

coincides with one of the surface- or volume-plasmon resonance frequencies of the column, assuming that its radius is much less than the wavelength in the outer isotropic medium. It is important that the energy flow pattern in the case of oblique incidence is essentially three-dimensional, in contrast to the two-dimensional pattern for normal incidence on the column [9]. Therefore, the behavior of the three-dimensional spatial structure of the Poynting-vector field in the case of oblique incidence actually requires special consideration.

Our work is organized as follows. In Section 2, we present the formulation of the problem and basic equations. In Section 3, we examine the field structures and the Poynting-vector patterns at the surface-plasmon resonance frequencies. Section 4 continues the analysis of Section 3 by considering the scattering at the resonances of the volume type. Section 5 presents conclusions of the performed analysis. Details of some mathematical derivations are contained in Appendix A.

2. FORMULATION OF THE PROBLEM AND BASIC EQUATIONS

Consider an infinitely long column of radius a that is located in free space and filled with a cold collisionless magnetoplasma. It is assumed that an external static magnetic field $\mathbf{B}_0$ is parallel to the column axis, which is aligned with the z axis of a cylindrical coordinate system $(\rho,\ \phi,\ z)$. A monochromatic H-polarized plane electromagnetic wave with angular frequency ω is incident on the column at an angle θ_0 to the z axis. Without loss of generality, it can be assumed that in the incident wave, in which the H_z component is nonzero, the electric field has the only nonzero E_x component, as is shown in Fig. 1. Then the electric and magnetic fields in the incident wave can be written, with $\exp(i\omega t)$ time dependence dropped, as

$$\mathbf{E}^{(i)} = \mathbf{E}_0^{(i)} \exp\left[-ik_0(qy+pz)\right], \quad \mathbf{H}^{(i)} = \mathbf{H}_0^{(i)} \exp\left[-ik_0(qy+pz)\right]. \tag{1}$$

Hereafter, k_0 is the wave number in free space; $p = \cos\theta_0$ and $q = \sin\theta_0$ are the normalized (to k_0) longitudinal and transverse components of the wave vector $\mathbf{k}$ in the incident wave, respectively; superscript (i) denotes the incident wave. The magnetic field in this wave is related to the electric field by the formula $\mathbf{H}_0^{(i)} = Z_0^{-1}(q\mathbf{y}_0 + p\mathbf{z}_0) \times \mathbf{E}_0^{(i)}$, where $\mathbf{E}_0^{(i)} = -E_0\mathbf{x}_0$, Z_0 is the impedance of free space, and $\mathbf{x}_0$, $\mathbf{y}_0$, and $\mathbf{z}_0$ are the unit vectors of the Cartesian coordinate system. In what follows, all the field quantities will be normalized to the electric-field amplitude E_0.

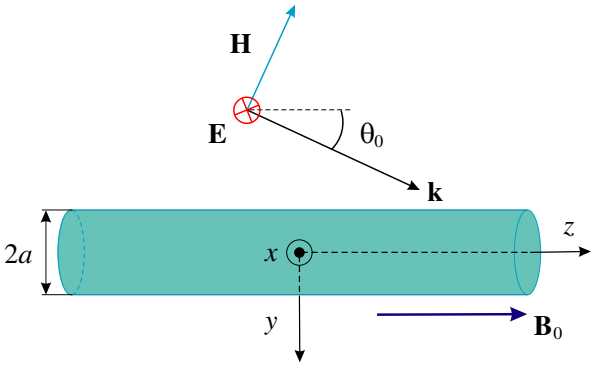

Figure 1. Geometry of the problem.

As is known [10], the cold collisionless magnetoplasma is described by the dielectric permittivity tensor of the following form:

$$\boldsymbol{\varepsilon} = \epsilon_0 \begin{pmatrix} \varepsilon & -ig & 0 \\ ig & \varepsilon & 0 \\ 0 & 0 & \eta \end{pmatrix}. \tag{2}$$

Here, ϵ_0 is the electric constant, and the tensor elements can be written as

$$\varepsilon = 1 - \frac{\omega_p^2}{\omega^2 - \omega_H^2}, \quad g = \frac{\omega_p^2 \omega_H}{\left(\omega^2 - \omega_H^2\right)\omega}, \quad \eta = 1 - \frac{\omega_p^2}{\omega^2}, \tag{3}$$

where ω_H and ω_p are the gyrofrequency and the plasma frequency of electrons, respectively. Note that in tensor elements (3), we have neglected the contribution of ions. This is possible under the condition $\omega \gg \omega_{\mathrm{LH}}$ [6], which is assumed throughout this work (here, ω_{LH} is the lower hybrid resonance frequency). It is worth mentioning that the element ε of tensor (2) is then written as $\varepsilon = (\omega^2 - \omega_{\mathrm{UH}}^2)/(\omega^2 - \omega_H^2)$ and vanishes at $\omega = \omega_{\mathrm{UH}}$, where $\omega_{\mathrm{UH}} = (\omega_p^2 + \omega_H^2)^{1/2}$ is the upper hybrid resonance frequency.

The problem of scattering of a plane electromagnetic wave by the column filled with a magnetoplasma is reduced to finding solutions of the Maxwell equations in cylindrical coordinates inside the plasma column (for $\rho < a$) and in free space (for $\rho > a$). The solutions should satisfy the boundary conditions for the tangential field components at the column surface $\rho = a$. Note that in the case of oblique incidence, the total field inside the plasma column and the scattered field in free space are hybrid and comprise all six components, including those which are absent in the incident wave.

The electromagnetic field can be represented in terms of the azimuthal harmonics as

$$\mathbf{E} = \sum_{m=-\infty}^{\infty} \mathbf{E}_m \exp\left[-i(m\phi + k_0 p z)\right], \quad \mathbf{H} = \sum_{m=-\infty}^{\infty} \mathbf{H}_m \exp\left[-i(m\phi + k_0 p z)\right], \tag{4}$$

where m is the azimuthal index ($m = 0, \pm 1, \pm 2, \ldots$). In turn, the quantities $\mathbf{E}_m$ and $\mathbf{H}_m$ can be expressed via their longitudinal components $E_{m,z}$ and $H_{m,z}$, respectively, which depend only on ρ and satisfy the following equations in the plasma medium [6, 11]:

$$\hat{L}_m E_{m,z} - k_0^2 \frac{\eta}{\varepsilon}\left(p^2 - \varepsilon\right) E_{m,z} = -ik_0^2 \frac{g}{\varepsilon} p Z_0 H_{m,z}, \tag{5}$$

$$\hat{L}_m H_{m,z} - k_0^2 \left(p^2 + \frac{g^2}{\varepsilon} - \varepsilon\right) H_{m,z} = ik_0^2 \frac{g}{\varepsilon} \eta p Z_0^{-1} E_{m,z}, \tag{6}$$

where

$$\hat{L}_m = \frac{d^2}{d\rho^2} + \frac{1}{\rho}\frac{d}{d\rho} - \frac{m^2}{\rho^2}.$$

The transverse components $E_{m,\rho}$, $E_{m,\phi}$, $H_{m,\rho}$, and $H_{m,\phi}$ of $\mathbf{E}_m$ and $\mathbf{H}_m$ are expressed via the longitudinal components $E_{m,z}$ and $H_{m,z}$ as follows [6]:

$$E_{m,\rho} = A\left\{ipg\frac{m}{\rho}E_{m,z} + ip\left(\varepsilon - p^2\right)\frac{dE_{m,z}}{d\rho} + \left(\varepsilon - p^2\right)\frac{m}{\rho}Z_0 H_{m,z} + gZ_0\frac{dH_{m,z}}{d\rho}\right\}, \tag{7}$$

$$E_{m,\phi} = A\left\{p\left(\varepsilon - p^2\right)\frac{m}{\rho}E_{m,z} + pg\frac{dE_{m,z}}{d\rho} - ig\frac{m}{\rho}Z_0 H_{m,z} - i\left(\varepsilon - p^2\right)Z_0\frac{dH_{m,z}}{d\rho}\right\}, \tag{8}$$

$$H_{m,\rho} = A\left\{\left[g^2 - \varepsilon\left(\varepsilon - p^2\right)\right]\frac{m}{\rho}Z_0^{-1}E_{m,z} - p^2 g Z_0^{-1}\frac{dE_{m,z}}{d\rho} + ipg\frac{m}{\rho}H_{m,z} + ip\left(\varepsilon - p^2\right)\frac{dH_{m,z}}{d\rho}\right\}, \tag{9}$$

$$H_{m,\phi} = A\left\{ip^2 g\frac{m}{\rho}Z_0^{-1}E_{m,z} - i\left[g^2 - \varepsilon\left(\varepsilon - p^2\right)\right]Z_0^{-1}\frac{dE_{m,z}}{d\rho} + p\left(\varepsilon - p^2\right)\frac{m}{\rho}H_{m,z} + pg\frac{dH_{m,z}}{d\rho}\right\}, \tag{10}$$

where $A = k_0^{-1}[g^2 - (p^2 - \varepsilon)^2]^{-1}$.

To obtain equations for the longitudinal field components and expressions for the corresponding transverse components outside the column, one should put $\varepsilon = 1$, $g = 0$, and $\eta = 1$ in Equations (5)–(10).

The field outside the column is a superposition of the scattered and incident-wave fields. The azimuthal harmonics of the longitudinal components of the field in the incident plane wave are written as

$$E_{m,z}^{(i)} = 0, \quad H_{m,z}^{(i)} = Z_0^{-1} q J_m(k_0 q \rho), \tag{11}$$

where J_m is a Bessel function of the first kind of order m.

The scattered field, denoted by the superscript (s), is also written in terms of cylindrical functions and has the following longitudinal components:

$$E_{m,z}^{(s)} = D_m^{(E)} q H_m^{(2)}(k_0 q \rho), \quad H_{m,z}^{(s)} = Z_0^{-1} D_m^{(H)} q H_m^{(2)}(k_0 q \rho), \tag{12}$$

where $H_m^{(2)}$ is a Hankel function of the second kind of order m, and $D_m^{(E)}$ and $D_m^{(H)}$ are the scattering coefficients corresponding to the azimuthal index m. It can easily be verified that the longitudinal components (12) satisfy Equations (5) and (6) if $\varepsilon = \eta = 1$ and $g = 0$.

The components of the field inside the column, which are solutions of Equations (5) and (6), are represented in the form

$$E_{m,z}^{(t)} = -\frac{i}{\eta}\sum_{k=1}^{2} B_m^{(k)} n_k q_k J_m(k_0 q_k \rho), \quad H_{m,z}^{(t)} = Z_0^{-1}\sum_{k=1}^{2} B_m^{(k)} q_k J_m(k_0 q_k \rho). \tag{13}$$

Here, superscript (t) denotes the field transmitting to the column, and $B_m^{(1)}$ and $B_m^{(2)}$ are the amplitude coefficients corresponding to the azimuthal index m for the field inside the column,

$$n_k = -\frac{\varepsilon}{pg}\left(p^2 + q_k^2 + \frac{g^2}{\varepsilon} - \varepsilon\right), \quad k = 1, 2, \tag{14}$$

and the normalized (to k_0) transverse wave numbers q_1 and q_2 in the magnetoplasma filling the column are related to p by the formula

$$q_k = \frac{1}{\sqrt{2}}\left\{\varepsilon - \frac{g^2}{\varepsilon} + \eta - \left(\frac{\eta}{\varepsilon} + 1\right)p^2 - \left(\frac{\eta}{\varepsilon} - 1\right)(-1)^k \left[\left(p^2 - P_b^2\right)\left(p^2 - P_c^2\right)\right]^{1/2}\right\}^{1/2}, \tag{15}$$

where

$$P_{b,c} = \left\{\varepsilon - (\eta + \varepsilon)\frac{g^2}{(\eta - \varepsilon)^2} + \frac{2\chi_{b,c}}{(\eta - \varepsilon)^2}\left[\varepsilon g^2 \eta\left(g^2 - (\eta - \varepsilon)^2\right)\right]^{1/2}\right\}^{1/2} \tag{16}$$

with $\chi_b = -\chi_c = -1$.

The presence of two transverse wave numbers q_1 and q_2 in a magnetoplasma, which correspond to the same longitudinal wave number p, is related to anisotropic properties of a magnetized plasma medium, in which two normal waves, ordinary and extraordinary, are excited by an obliquely incident plane electromagnetic wave. This circumstance represents an essential difference of the problem discussed herein from that in [9], where an H-polarized plane wave incident normally on the gyrotropic column was considered and only one (extraordinary) wave could be excited inside the column.

The coefficients $B_m^{(1,2)}$, $D_m^{(E)}$, and $D_m^{(H)}$ are determined from the conditions of continuity of the tangential field components at the surface of the column:

$$\begin{aligned} E_{m,\phi}^{(t)} &= E_{m,\phi}^{(i)} + E_{m,\phi}^{(s)}, \quad E_{m,z}^{(t)} = E_{m,z}^{(i)} + E_{m,z}^{(s)}, \\ H_{m,\phi}^{(t)} &= H_{m,\phi}^{(i)} + H_{m,\phi}^{(s)}, \quad H_{m,z}^{(t)} = H_{m,z}^{(i)} + H_{m,z}^{(s)}. \end{aligned} \tag{17}$$

The procedure of satisfying conditions (17) yields an inhomogeneous system of four linear equations for the above-mentioned coefficients. The expressions for the coefficients $B_m^{(1,2)}$, $D_m^{(E)}$, and $D_m^{(H)}$ turn out to be very cumbersome and are not written here for the sake of brevity. Some details of the derivation of these coefficients are given in Appendix A. Their analysis shows that the absolute values of the coefficients $D_m^{(E)}$ and $D_m^{(H)}$ become maximum at some resonant frequencies, at which enhanced scattering occurs from the column. These frequencies correspond to plasmon resonances of the column. Strictly speaking, the frequencies at which the absolute values of the scattering coefficients reach their maxima are not exactly equal to each other, but the difference between the respective frequencies is less than or about the resonance linewidth, which is very small. A similar situation occurs for the coefficients $B_m^{(1,2)}$, whose absolute values become maximum at frequencies that are extremely close to the resonant frequencies of the scattering coefficients. The above-described slight differences are explained by the fact that the coefficients $B_m^{(1,2)}$, $D_m^{(E)}$, and $D_m^{(H)}$ represent ratios with a common denominator, which is given by the determinant of the system of equations for these coefficients, and different numerators (see Appendix A). Since the corresponding numerators are slowly varying smooth functions of frequency compared with the denominator, which sharply varies near each of its minima, the frequency positions of these minima will be adopted as the frequencies of plasmon resonances throughout this work. We

emphasize that in what follows, we will consider only the resonance scattering when the frequency ω coincides with some of the plasmon resonance frequencies.

To analyze the behavior of the energy flow, we should calculate the patterns of the time-averaged Poynting vector which is given by the well-known relation $\mathbf{S} = (1/2)\mathrm{Re}(\mathbf{E} \times \mathbf{H}^*)$, where the asterisk denotes complex conjugation. For convenience, the quantity $\mathbf{S}$ normalized to the magnitude of the Poynting vector $\mathbf{S}^{(i)}$ in the incident wave is used throughout this work. For better clarity, we will present the three-dimensional patterns of the normalized Poynting-vector field lines along with the two-dimensional plots showing the projections $\mathbf{S}_\perp$ and S_z of the Pointing vector onto the xy plane and the z axis, respectively, as functions of the transverse coordinates x and y.

3. SCATTERING AT THE SURFACE PLASMON RESONANCES

As is known, the quasistatic surface plasmon resonances exist in the case of electrically small scatterers. For a magnetized plasma column, this implies the fulfillment of the conditions $k_0 a \ll 1$ and $k_0|q_{1,2}|a \ll 1$. The surface-plasmon resonances will further be denoted as SP_m, and the respective resonant frequencies as $\omega_{\mathrm{SP},m}$. Among all surface plasmon resonances, the resonances with the azimuthal indices $m = \pm 1$ are the most important in the case considered. It is evident that the corresponding resonant frequencies depend on the incidence angle θ_0. In the case $a \to 0$, the resonant frequencies for normal incidence ($\theta_0 = \pi/2$) are described by the expression [12–14]

$$\omega_{\mathrm{SP},\pm 1} = \left[\left(2\omega_p^2 + \omega_H^2\right)^{1/2} \pm \omega_H\right]/2. \tag{18}$$

In the absence of an external magnetic field, this formula gives the well-known result $\omega_{\mathrm{SP},\pm 1} = \omega_p/\sqrt{2}$ for the surface-plasmon resonance frequency of an isotropic cylinder, which is independent of the sign of the azimuthal index.

For an arbitrary incidence angle θ_0, the frequencies $\omega_{\mathrm{SP},\pm 1}$ as functions of θ_0 can be found only numerically. Numerical calculations were performed for the dimensionless parameters $\omega_p a/c = 0.188$ and $\omega_p/\omega_H = 8.02$. On the one hand, the use of these values ensures the clarity of the forthcoming figures. On the other hand, the chosen parameters can easily be realized if, e.g., the plasma column is created by an RF discharge under laboratory conditions (see, e.g., [15–17]). Fig. 2 shows the resonant frequencies $\omega_{\mathrm{SP},-1}$ and $\omega_{\mathrm{SP},1}$ as functions of the parameter $p = \cos\theta_0$, as well as the corresponding dependences of the absolute values of the scattering coefficients $D_1^{(E)}$ and $D_1^{(H)}$ at $\omega = \omega_{\mathrm{SP},1}$. The dependences of $|D_{-1}^{(E)}|$ and $|D_{-1}^{(H)}|$ on p for $\omega = \omega_{\mathrm{SP},-1}$ almost coincide with the corresponding results in

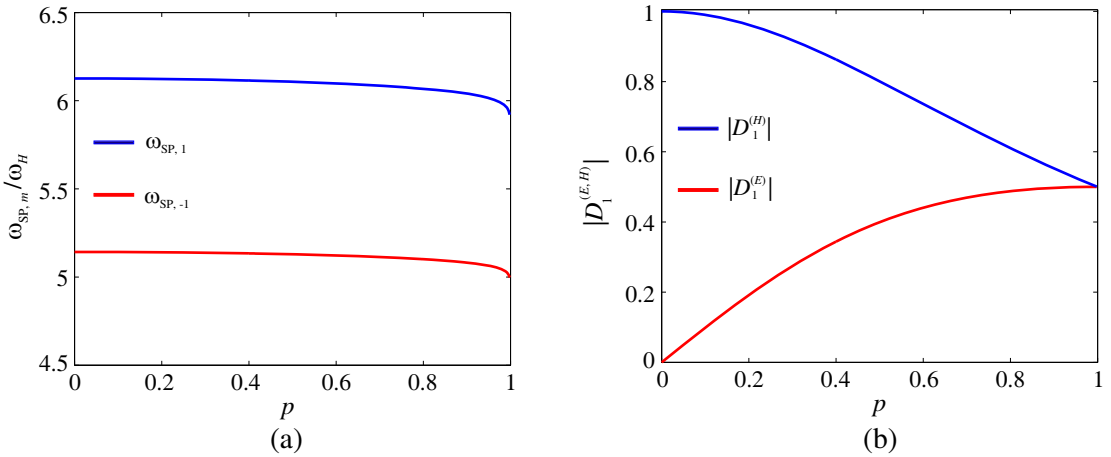

Figure 2. (a) Resonant frequencies $\omega_{\mathrm{SP},\pm 1}$ and (b) the absolute values of the scattering coefficients $D_1^{(E)}$ and $D_1^{(H)}$ at the frequency $\omega = \omega_{\mathrm{SP},1}$ as functions of the longitudinal wave number p for $\omega_p a/c = 0.188$ and $\omega_p/\omega_H = 8.02$.

Fig. 2(b) and, therefore, are not given here in the interests of brevity. Note that a variation in p from zero to unity in Fig. 2 corresponds to variation in the incidence angle from $\theta_0 = \pi/2$ to $\theta_0 = 0$. It is seen in Fig. 2(a) that the resonant frequencies $\omega_{\mathrm{SP},-1}$ and $\omega_{\mathrm{SP},1}$ depend on p only slightly, except for the region $p \lesssim 1$. This fact allows one to use formula (18) as a good approximation for $\omega_{\mathrm{SP},\pm 1}$ at almost all incidence angles, excluding only the case of grazing incidence. Another interesting feature is that the absolute values of the coefficients $D_1^{(E)}$ and $D_1^{(H)}$ vary from zero and unity, respectively, at $p = 0$, when $\theta_0 = \pi/2$, to 0.5 at $p = 1$ when $\theta_0 = 0$. The same behavior is observed for the absolute values of the corresponding scattering coefficients with the azimuthal index $m = -1$.

Now, as an example, we present the plots of the real and imaginary parts of the coefficients $D_1^{(E)}$ and $D_1^{(H)}$ as functions of ω and p. On the corresponding plots of Fig. 3, one can easily see the traces showing the relation of the surface-plasmon resonance frequency $\omega_{\mathrm{SP},1}$ to the longitudinal wave number p. It follows from Figs. 3(a) and 3(c) that at the resonant frequency, the real part of the coefficient $D_1^{(E)}$ passes through zero, whereas the imaginary part of this coefficient reaches its maximum in absolute value, except for the case $p = 0$ where $D_1^{(E)} = 0$. On the contrary, at the same resonant frequency, the real part of the coefficient $D_1^{(H)}$ is maximum in absolute value, while the imaginary part of $D_1^{(H)}$ passes through zero, as is seen in Figs. 3(b) and 3(d). Thus, we can state that at the surface-plasmon resonance frequency, the coefficient $D_1^{(E)}$ is purely imaginary, whereas the coefficient $D_1^{(H)}$ is purely real. The above features are evidently indicative of a $\pi/2$ phase shift between $D_1^{(E)}$ and $D_1^{(H)}$. The zero value of the coefficient $D_1^{(E)}$ for normal incidence, in which case $D_1^{(H)} = \mathrm{Re}D_1^{(H)} = -1$ at $\omega = \omega_{\mathrm{SP},1}$, means that the scattered field outside the cylinder and the total field in the inner region $\rho < a$ have the same polarization as the incident H wave. In the case of oblique incidence, both these fields become hybrid, i.e., have all six components. Indeed, as is evident from Equations (5)–(10), the total field inside the plasma column is always hybrid if $p \neq 0$. Hence, the scattered field must also be hybrid, which stipulates the nonzero value of $D_1^{(E)}$ as well as the other related features observed in the behavior of

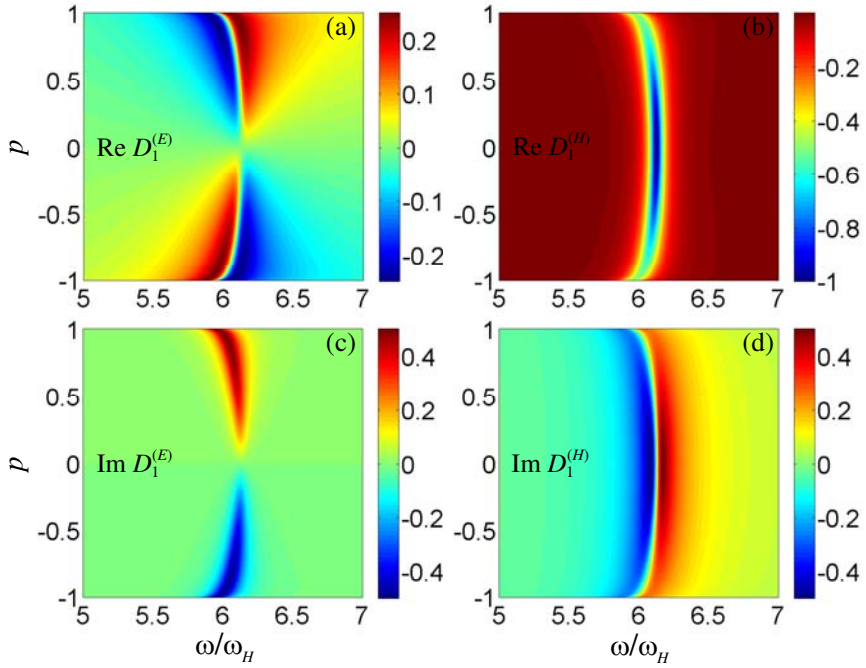

Figure 3. (a), (b) Real and (c), (d) imaginary parts of the scattering coefficients $D_1^{(E)}$ and $D_1^{(H)}$ as functions of the longitudinal wave number and frequency. The same parameters $\omega_p a/c$ and ω_p/ω_H as in Fig. 2.

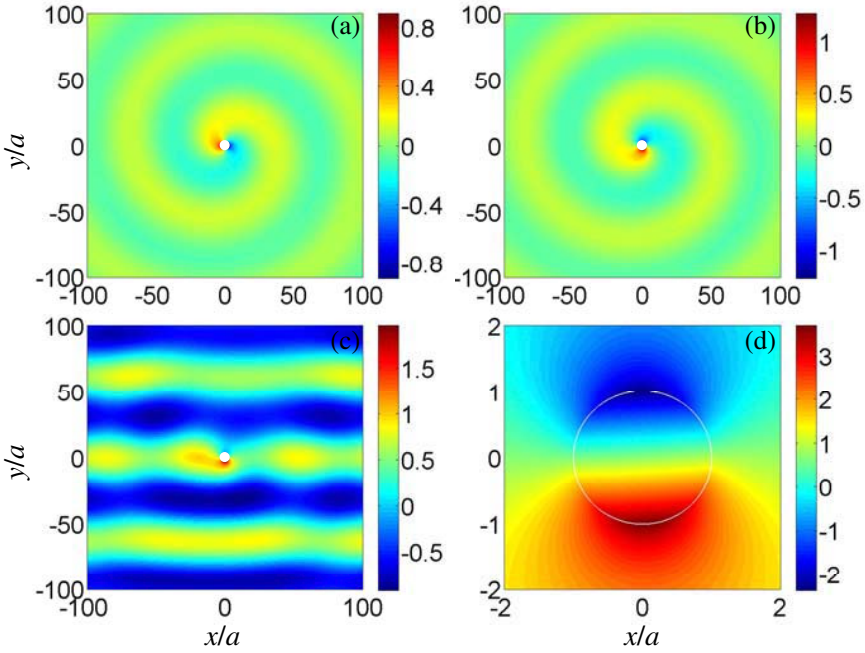

Figure 4. Snapshots of the normalized components (a) E_z and (b) Z_0H_z of the scattered field and the normalized component Z_0H_z of the total field (c) far from and (d) close to the plasma column at the resonant frequency $\omega = \omega_{\mathrm{SP},1}$ for the incidence angle $\theta_0 = \pi/4$. Other parameters are the same as in Fig. 2.

the scattering coefficients as functions of p.

The spatial structures of the scattered and total fields, which are normalized to the amplitude of the electric field in the incident wave, are illustrated by Fig. 4 plotted for the resonant frequency $\omega = \omega_{\mathrm{SP},1}$ and the incidence angle $\theta_0 = \pi/4$. In this case, $\omega_{\mathrm{SP},1}/\omega_H = 6.08$ and $p = 0.707$, provided that the values of other parameters are the same as in Fig. 2. The figure shows the plots of the components E_z and H_z, the latter being multiplied by the free-space impedance Z_0 for convenience of graphical representation. The snapshots of these components in the scattered field are depicted in Figs. 4(a) and 4(b), respectively. The behavior of the total field is shown by the snapshots of its longitudinal magnetic component H_z in the far zone of the plasma column and in its vicinity in Figs. 4(c) and 4(d), respectively. To avoid misunderstanding, we note that the field inside the plasma column is shown only in Fig. 4(d), in which the column boundary is marked by a thin circular white line. In other three panels of Fig. 4, the inner region of the column is shown white colored. It should be emphasized that the E_z component, which is absent in the incident field and appears in the scattered field, identically coincides with the longitudinal electric component in the total field and has a helical structure typical of scattering from gyrotropic objects, as is seen in Fig. 4(a). A similar structure is observed for the scattered magnetic field in Fig. 4(b). At the same time, the H_z component of the total field outside the column, which is determined by the superposition of the incident- and scattered-field contributions, has an essentially different structure. It is worth mentioning that at the frequency $\omega = \omega_{\mathrm{SP},-1}$ of the other dipolar surface-plasmon resonance, the helical structures of the corresponding field snapshots has the opposite untwisting direction and the values of the field components somewhat differ from those for the frequency $\omega = \omega_{\mathrm{SP},1}$, because all the field components are frequency dependent.

We now proceed to analysis of the energy flow patterns in the case of resonance scattering. Fig. 5 shows the magnitude (in color scale) and the spatial structure of field lines of the time-averaged Poynting vector $\mathbf{S}$ for the total field in the case where $\omega = \omega_{\mathrm{SP},1}$, $\theta_0 = \pi/4$, and the other parameters are the same as in Fig. 2. The behavior of the transverse (with respect to the column axis) component $\mathbf{S}_\perp$ of the vector $\mathbf{S}$ is illustrated by Fig. 5(a), in which the lines with arrows indicate the field lines and local directions of $\mathbf{S}_\perp$. This plot can be divided into three regions the boundaries of which are represented by

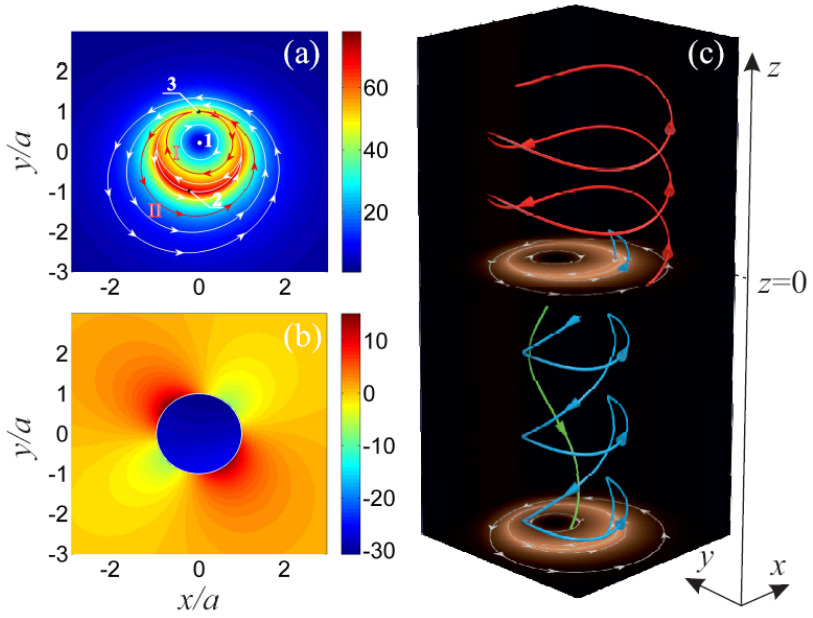

Figure 5. (a) Field lines and the magnitude of the transverse component $\mathbf{S}_\perp$ of the normalized Poynting vector, (b) the pattern of its longitudinal component S_z, and (c) the stereometric view of the Poynting-vector lines at the resonant frequency $\omega = \omega_{\mathrm{SP},1}$ for the incidence angle $\theta_0 = \pi/4$. Other parameters are the same as in Fig. 2.

red lines I and II. In the first region enclosed by the boundary I, the lines of $\mathbf{S}_\perp$ circulate around point 1 near the axis of the column. In the second region between the boundaries I and II, the adjacent lines of $\mathbf{S}_\perp$ in the vicinity of point 2 at the column surface have opposite directions. Note that the lines I and II have common point 3 on the surface of the column. It should be mentioned that the radial component S_ρ of the Poynting vector at the column surface is zero at points 2 and 3. In the third region in Fig. 5(a), which is located outside the boundary II, the lines of $\mathbf{S}_\perp$ circulate around the column in the direction opposite to that in the first region. Fig. 5(b) shows the longitudinal component S_z of the time-averaged normalized Poynting vector. It is seen in the figure that the S_z component inside the column is negative. Such behavior of S_z (i.e., $S_z < 0$) is also observed in some regions outside the column in close proximity to its surface. In other regions outside the column, $S_z > 0$. The above-described features of the energy flow pattern are attributed to the discontinuous behavior of the tangential component of the Poynting vector at the column surface, although the radial component S_ρ of this vector remains continuous for $\rho = a$. As a result, the Poynting-vector lines undergo refraction at the column surface similarly to that observed at the boundary of an isotropic cylinder [18, 19].

To clarify the three-dimensional behavior of the Poynting-vector field, Fig. 5(c) shows the stereometric view of the energy flow lines corresponding to the three regions mentioned above. All the lines presented in the figure originate in the plane $z = 0$. The green line in Fig. 5(c) corresponds to the first region in Fig. 5(a). It is evident that the respective energy flow is oriented predominantly along the negative direction of the z axis, which is also seen in Fig. 5(b). The blue line, for which S_z is mostly negative, and the red line, for which S_z is mostly positive, refer to the second and the third regions in Fig. 5(a), respectively. It is worth noting that in the case $p = 0$ where $S_z = 0$ and $\mathbf{S} = \mathbf{S}_\perp$, the Poynting-vector pattern inside the column and in its vicinity coincides qualitatively with the plot in Fig. 5(a).

It should be mentioned that despite the symmetry of the incident plane wave with respect to the yz plane, the patterns in Fig. 5 do not demonstrate such symmetry. This is explained by the gyrotropic (nonreciprocal) properties of the medium filling the scattering column. If we plot the Poynting-vector field lines for the surface-plasmon resonance frequency $\omega = \omega_{\mathrm{SP},-1}$, the resulting patterns will be almost symmetric to those shown in Fig. 5 with respect to the yz plane. Some asymmetry that can be observed

in such a case is explained by a change in the resonant frequency.

An important implication of the numerical results is that the magnitude of the Poynting vector near the boundary of a magnetized plasma column at the surface-plasmon resonance frequency significantly exceeds that in the incident wave, as well as in the case of resonance scattering from an isotropic plasma column. The region with enhanced energy-flow density has a well-pronounced crescent shape in Fig. 5(a). Interestingly, such a shape remains intact when passing from oblique to normal incidence, provided that the condition $\omega = \omega_{\mathrm{SP},\pm 1}$ is ensured for each incidence direction.

4. SCATTERING AT THE VOLUME PLASMON RESONANCES

We now consider scattering at plasmon resonances of the volume type. Their existence is related to the fact that in a homogeneous cold collisionless magnetoplasma, one of the transverse wave numbers q_1 and q_2 for a fixed p tends to infinity at a certain frequency if the latter lies in one of the so-called resonant frequency ranges [6]. If tensor elements (3) are used, there exist two resonant frequency ranges, namely, $\omega < \min\{\omega_H, \omega_p\}$ and $\max\{\omega_H, \omega_p\} < \omega < \omega_{\mathrm{UH}}$. We will focus on the latter frequency interval, which is usually called the upper hybrid range. In this range, the cylindrically shaped magnetoplasma for any azimuthal index m has an infinite number of resonances of the volume type even if the scatterer radius is much less than the wavelength in the outer isotropic medium. These resonances and their resonant frequencies will be denoted as $\mathrm{UH}_{m,n}$ and $\omega_{\mathrm{UH},m,n}$, respectively, where the index n ($n = 1, 2, \ldots$) labels the resonances in order of increasing resonant frequency for a fixed azimuthal index m. Note that the index n determines the number of field oscillations over the radial coordinate inside the plasma column. It turns out that the frequencies of such resonances lie slightly below the upper hybrid frequency ω_{UH} and are located more and more densely when approaching ω_{UH}. This is well seen in Fig. 6 which shows the plots of the real and imaginary parts of the coefficients $D_m^{(E)}$ and $D_m^{(H)}$ as functions of ω and p near the upper hybrid frequency ω_{UH} for $m = 0$ and the previously chosen values of the parameters $\omega_p a/c$ and ω_p/ω_H. As in Fig. 3, the traces in Fig. 6 represent the relation of the volume-plasmon resonance frequencies $\omega_{\mathrm{UH},0,n}$ to the longitudinal wave number p. It is evident that despite some quantitative

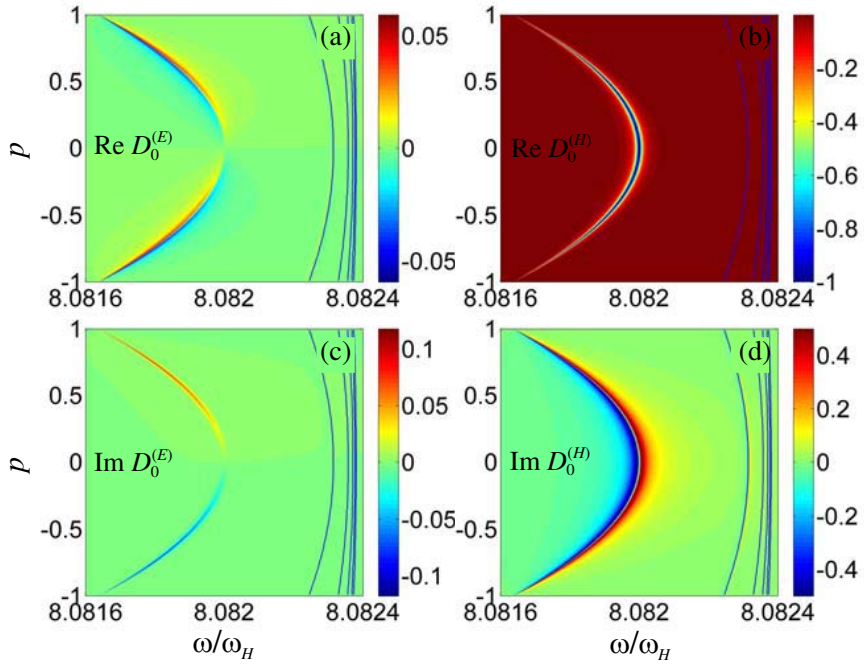

Figure 6. (a), (b) Real and (c), (d) imaginary parts of the scattering coefficients $D_0^{(E)}$ and $D_0^{(H)}$ as functions of the longitudinal wave number and frequency near the upper hybrid frequency ω_{UH} for $\omega_p a/c = 0.188$ and $\omega_p/\omega_H = 8.02$.

differences, the behavior of the scattering coefficients near the volume-plasmon resonant frequencies is qualitatively similar to that for the surface plasmon resonances. Note that the linewidths of the $\mathrm{UH}_{0,n}$ resonances are so small that the corresponding traces for $n = 2, \ldots, 6$ on the presented plots are seen as thin lines, which are shown blue colored in Fig. 6.

Since the field at the $\mathrm{UH}_{m,n}$ resonances is predominantly concentrated inside the plasma column, allowance for even a minor ohmic loss in the plasma immediately leads to a sharp decrease in the peak values of the scattering coefficients and, moreover, overlapping of the resonances that are closely located in the vicinity of the upper hybrid frequency ω_{UH}. Therefore, only the $\mathrm{UH}_{m,1}$ resonances, which are more distant from other resonances with the frequencies concentrated near ω_{UH}, apparently have practical value. In this respect, the $\mathrm{UH}_{0,1}$ resonance, which has the widest linewidth and the most distant frequency from ω_{UH}, seems fairly promising.

The snapshots of the field at this resonance are presented for the incidence angle $\theta_0 = \pi/4$ in Fig. 7. In this case, $\omega_{\mathrm{UH},0,1}/\omega_H = 8.0818$. It should be noted that at this resonance, the longitudinal magnetic-field component of the scattered field outside the column reaches its maximum absolute value at time instants at which the same component of the field inside the column is minimum in magnitude. In view of this, the H_z component of the total field inside the column in Fig. 7(d) corresponds to the time instant that differs by a quarter of the field period from the time instant chosen for plotting the other three panels of this figure, with the white-colored inner region of the column.

A typical feature of the $\mathrm{UH}_{m,n}$ resonances is the volume structure of the field inside the scatterer, which is well seen in Fig. 7(d). Moreover, this field is much greater than the scattered and incident-wave fields. Weak asymmetry in the pattern of Fig. 7(a) is explained by the contribution of the nonresonant azimuthal field harmonics, which are present in the total field along with the $m = 0$ resonant harmonic.

The structure of the energy flow at the resonant frequency $\omega = \omega_{\mathrm{UH},0,1}$ is shown in Figs. 8 and 9 for $\theta_0 = \pi/4$ and the same parameters $\omega_p a/c$ and ω_p/ω_H as in the preceding figures. Since the Poynting-vector magnitude inside the column is much greater than that in the surrounding medium, we cannot use the same scale for representing the Poynting-vector behavior in the inner and outer regions. Therefore,

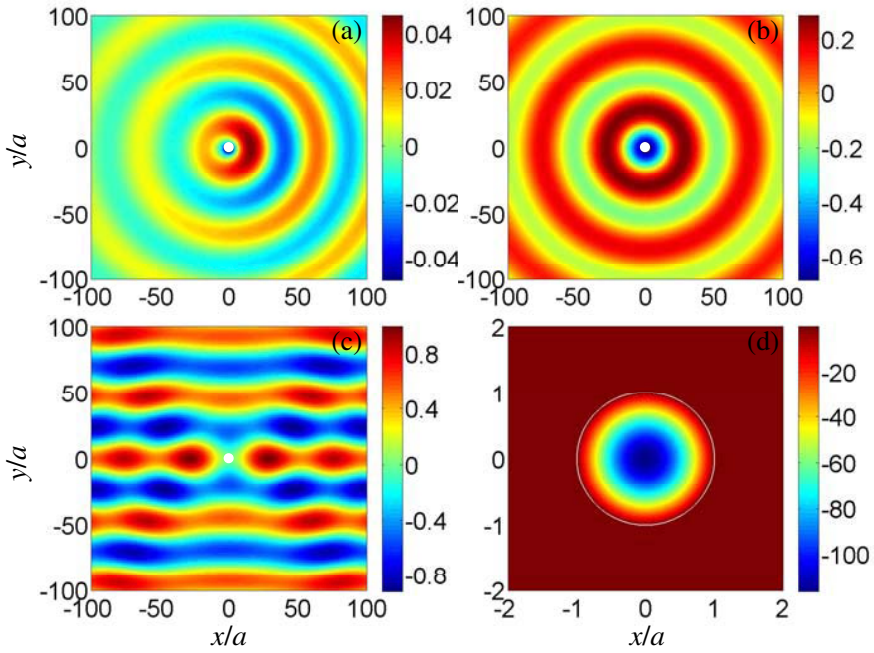

Figure 7. Snapshots of the normalized components (a) E_z and (b) $Z_0 H_z$ of the scattered field and the normalized component $Z_0 H_z$ of the total field (c) far from and (d) inside the plasma column at the resonant frequency $\omega = \omega_{\mathrm{UH},0,1}$ for the incidence angle $\theta_0 = \pi/4$. The last panel corresponds to the time instant differing by a quarter of the field period from the time instant chosen for plotting the other panels. The parameters $\omega_p a/c$ and ω_p/ω_H are the same as in Fig. 6.

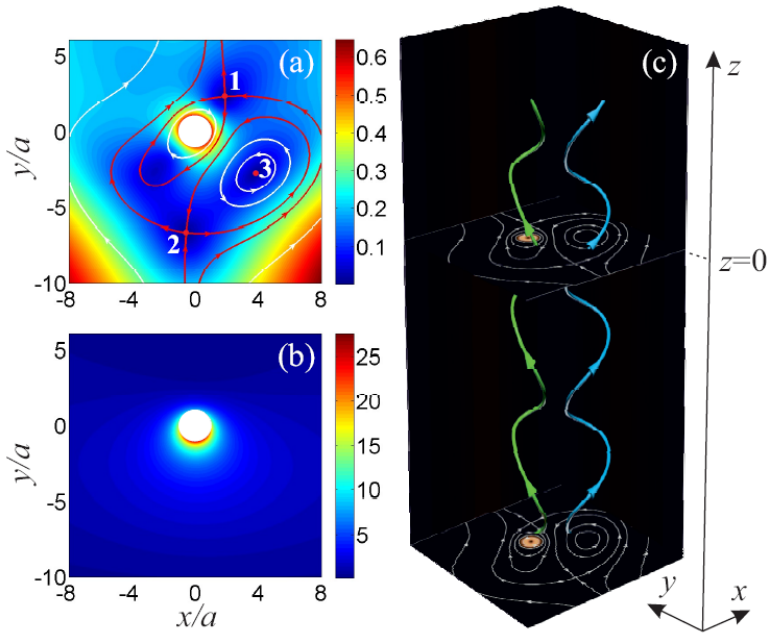

Figure 8. (a) Field lines and the magnitude of the transverse component $\mathbf{S}_\perp$ of the Poynting vector, (b) the pattern of its longitudinal component S_z, and (c) the stereometric view of the Poynting-vector lines outside the plasma column at the resonant frequency $\omega = \omega_{\mathrm{UH},0,1}$ for the incidence angle $\theta_0 = \pi/4$. Other parameters are the same as in Fig. 6.

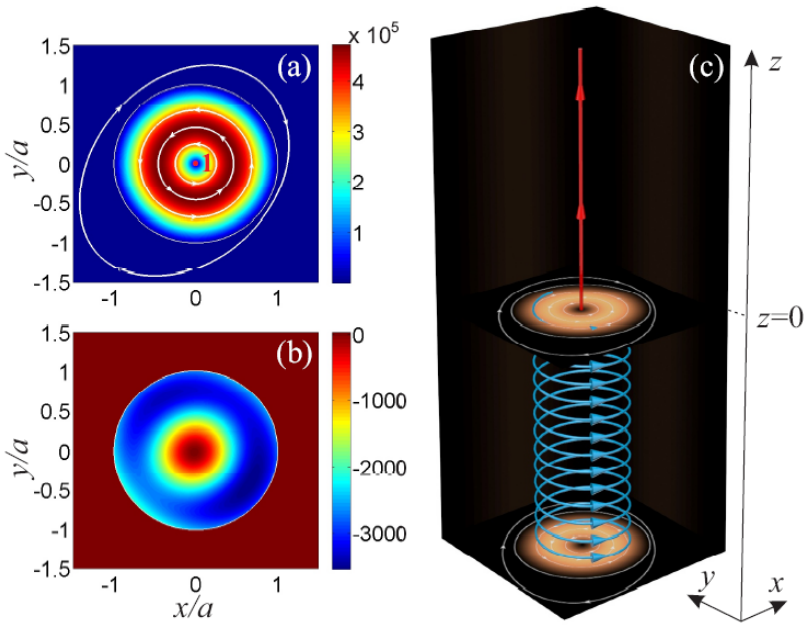

Figure 9. The same as in Fig. 8, but for the inner region of the plasma column and in its close vicinity.

Figs. 8(a) and 8(b) show the patterns of the transverse and longitudinal components of the Poynting vector only in the outer region. The behavior of these components inside the column is shown on another scale in Figs. 9(a) and 9(b).

It is seen that outside the column, the Poynting vector has the positive longitudinal component

S_z, which is illustrated by, e.g., the green and blue lines in Fig. 8(c). Inside the column, $S_z < 0$ almost everywhere, except for the near-axis region in which $S_z > 0$, as is shown by the blue and red lines in Fig. 9(c), respectively. Since $|S_z| \ll |\mathbf{S}_\perp|$ in the region $\rho \lesssim a$, the pitch of a helix showing the Poynting-vector field line inside the column turns out to be very small in Fig. 9(c). In the case $p = 0$, the Poynting-vector pattern inside the column remains almost the same as in Fig. 9(a), i.e., energy will circulate along the closed trajectories around the center point. Finally, we note that asymmetry of the Poynting-vector patterns with respect to the yz plane in Figs. 8 and 9 is explained by the same reason as for Fig. 5, namely, the gyrotropic properties of the magnetoplasma in the column.

5. CONCLUSION

We have analyzed the total field and the energy flow behavior in the case of resonance scattering of an obliquely incident H-polarized plane electromagnetic wave by a magnetized plasma column whose radius is much smaller than the wavelength in the surrounding isotropic medium. It is shown that at the surface plasmon resonance, the Poynting-vector magnitude near the boundary of a gyrotropic cylinder is much greater than that for an incident wave. Moreover, it has been established that a significant increase in the field and the Poynting-vector magnitude inside a magnetized plasma column at the frequencies of volume resonances can take place compared with the case of surface plasmon resonances. In addition, the sign reversal of the longitudinal energy-flow component is found to occur when passing across the boundary between the inner region of such a column and the surrounding medium. The results obtained open up a variety of possibilities for controlling the energy flow by tuning the parameters of the plasma column. The easiest way for doing this is apparently by varying an external magnetic field, although variation in other parameters can also be used.

Despite the fact that we performed our numerical calculations for the column filled with a magnetoplasma, the general features of wave scattering, which have been revealed during this analysis, will be observed for scattering from arbitrary gyrotropic cylindrical objects whose dielectric permittivity can be described by the tensor of general form (2). Even if the expressions for the tensor elements differ from those used in this work, the scattering properties of cylindrical gyrotropic structures will evidently demonstrate qualitatively similar behavior, regardless of the physical nature of particular media filling such scatterers.

ACKNOWLEDGMENT

This work was supported by the Russian Science Foundation (project No. 14-12-00510). Some numerical codes used for calculations were developed under support from the President Grant MK-4688.2014.2 for young Russian scientists, the Russian Foundation for Basic Research (project No. 14-01-31280), and the Government of the Russian Federation (project No. 14.B25.31.0008).

APPENDIX A. COEFFICIENTS FOR THE FIELDS SCATTERED FROM AND TRANSMITTED TO THE MAGNETIZED PLASMA CYLINDER

We present here the salient steps of the derivation of the coefficients $B_m^{(1,2)}$, $D_m^{(E)}$, and $D_m^{(H)}$. The boundary conditions (17) can thus be represented in matrix form:

$$\boldsymbol{S}_m \cdot \mathbf{C}_m = \mathbf{W}_m. \tag{A1}$$

The elements of the matrix $\boldsymbol{S}_m$ and of the vectors $\mathbf{C}_m$ and $\mathbf{W}_m$ are written as follows:

$$\begin{aligned}
S_{m,11} &= \frac{n_1}{\eta} Q_1 J_m(Q_1), \quad S_{m,12} = \frac{n_2}{\eta} Q_2 J_m(Q_2), \quad S_{m,13} = -iQH_m^{(2)}(Q), \quad S_{m,14} = 0,\\
S_{m,21} &= Q_1 J_m(Q_1), \quad S_{m,22} = Q_2 J_m(Q_2), \quad S_{m,23} = 0, \quad S_{m,24} = -QH_m^{(2)}(Q),\\
S_{m,31} &= J_m^{(1)}, \quad S_{m,32} = J_m^{(2)}, \quad S_{m,33} = i\frac{mp}{Q} H_m^{(2)}(Q), \quad S_{m,34} = -\mathcal{H}_m,\\
S_{m,41} &= n_1 \tilde{J}_m^{(1)}, \quad S_{m,42} = n_2 \tilde{J}_m^{(2)}, \quad S_{m,43} = -i\mathcal{H}_m, \quad S_{m,44} = \frac{mp}{Q} H_m^{(2)}(Q),
\end{aligned}$$

$$C_{m,1} = B_m^{(1)}, \quad C_{m,2} = B_m^{(2)}, \quad C_{m,3} = D_m^{(E)}, \quad C_{m,4} = D_m^{(H)},$$
$$W_{m,1} = 0, \quad W_{m,2} = QJ_m(Q), \quad W_{m,3} = \mathcal{J}_m, \quad W_{m,4} = -\frac{mp}{Q}J_m(Q). \tag{A2}$$

Here,

$$\mathcal{J}_m = J_{m+1}(Q) - \frac{m}{Q}J_m(Q), \quad \mathcal{H}_m = H_{m+1}^{(2)}(Q) - \frac{m}{Q}H_m^{(2)}(Q), \quad Q = k_0aq,$$
$$J_m^{(k)} = J_{m+1}(Q_k) + \frac{m\alpha_k}{Q_k}J_m(Q_k), \quad \tilde{J}_m^{(k)} = J_{m+1}(Q_k) - \frac{m\beta_k}{Q_k}J_m(Q_k), \quad Q_k = k_0aq_k,$$
$$\alpha_k = \left(p^2 + q_k^2 - \varepsilon\right)g^{-1} - 1, \quad \beta_k = pn_k^{-1} + 1, \quad k = 1, 2, \tag{A3}$$

and the other notations are defined in Equations (14)–(16).

We denote the determinant of the matrix $\boldsymbol{S}_m$ by Δ_m. Let $\Delta_m^{(l)}$ be the determinant of a matrix $\boldsymbol{S}_m^{(l)}$ $(l = 1, \ldots, 4)$ that is obtained by the replacement of the lth column of the matrix $\boldsymbol{S}_m$ by the elements of the vector $\mathbf{W}_m$, i.e., $S_{m,ij}^{(l)} = S_{m,ij}$ for $j \neq l$ and $S_{m,il}^{(l)} = W_{m,i}$, where $i, j = 1, \ldots, 4$. Then the coefficients $B_m^{(1,2)}$, $D_m^{(E)}$, and $D_m^{(H)}$ are calculated in a standard manner as

$$B_m^{(1)} = \Delta_m^{(1)}/\Delta_m, \quad B_m^{(2)} = \Delta_m^{(2)}/\Delta_m, \quad D_m^{(E)} = \Delta_m^{(3)}/\Delta_m, \quad D_m^{(H)} = \Delta_m^{(4)}/\Delta_m. \tag{A4}$$

REFERENCES

1. Felsen, L. B. and N. Marcuvitz, *Radiation and Scattering of Waves*, Prentice-Hall, Englewood-Cliffs, 1973.
2. Armelles, G., A. Cebollada, A. García-Martín, and M. Ujué González, "Magnetoplasmonics: Combining magnetic and plasmonic functionalities," *Adv. Optical Mater.*, Vol. 1, No. 1, 10–35, 2013.
3. Wang, Z., Y. D. Chong, J. D. Joannopoulos, and M. Soljačić, "Reflectionfree one-way edge modes in a gyromagnetic photonic crystal," *Phys. Rev. Lett.*, Vol. 100, No. 1, 013905, 2008.
4. Davoyan, A. R. and N. Engheta, "Nonreciprocal rotating power flow within plasmonic nanostructures," *Phys. Rev. Lett.*, Vol. 111, No. 4, 047401, 2013.
5. Davoyan, A. R. and N. Engheta, "Nanoscale plasmonic circulator," *New J. Phys.*, Vol. 15, No. 8, 083054, 2013.
6. Kondrat'ev, I. G., A. V. Kudrin, and T. M. Zaboronkova, *Electrodynamics of Density Ducts in Magnetized Plasmas*, Gordon and Breach, Amsterdam, 1999.
7. Kudrin, A. V., N. M. Shkokova, O. E. Ferencz, and T. M. Zaboronkova, "Whistler wave radiation from a pulsed loop antenna located in a cylindrical duct with enhanced plasma density," *Phys. Plasmas*, Vol. 21, No. 11, 112115, 2014.
8. Kudrin, A. V., A. S. Zaitseva, T. M. Zaboronkova, and S. S. Zilitinkevich, "Current distribution and input impedance of a strip loop antenna located on the surface of a circular column filled with a resonant magnetoplasma," *Progress In Electromagnetics Research B*, Vol. 55, 241–256, 2013.
9. Ivoninsky, A. V., V. A. Es'kin, and A. V. Kudrin, "The energy flow behavior during the resonance scattering of a plane electromagnetic wave by a magnetized plasma column," *Nizhny Novgorod Univ. Bull.*, No. 1, Pt. 2, 141–149, 2014.
10. Ginzburg, V. L., *The Propagation of Electromagnetic Waves in Plasmas*, Pergamon Press, Oxford, 1970.
11. Kudrin, A. V., E. Yu. Petrov, G. A. Kyriacou, and T. M. Zaboronkova, "Electromagnetic radiation from sources embedded in a cylindrically stratified unbounded gyrotropic medium," *Progress In Electromagnetics Research B*, Vol. 12, 297–331, 2009.
12. Crawford, F. W., G. S. Kino, and A. B. Cannara, "Dipole resonances of a plasma in a magnetic field," *J. Appl. Phys.*, Vol. 34, No. 11, 3168–3175, 1963.
13. Seshadri, S. R., "Plane-wave scattering by a magnetoplasma cylinder," *Electron. Lett.*, Vol. 1, No. 9, 256–258, 1965.

14. Gildenburg, V. B. and G. A. Markov, "The resonances of a gas-discharge plasma in a magnetic field," *Radiophys. Quantum Electron.*, Vol. 11, No. 5, 446–448, 1968.
15. Chen, F. F. and R. W. Boswell, "Helicons — The past decade," *IEEE Trans. Plasma Sci.*, Vol. 25, No. 6, 1245–1257, 1997.
16. Carter, M. D., F. W. Baity, Jr., G. C. Barber, R. H. Goulding, Y. Mori, D. O. Sparks, K. F. White, E. F. Jaeger, F. R. Chang-Díaz, and J. P. Squire, "Comparing experiments with modeling for light ion helicon plasma sources," *Phys. Plasmas*, Vol. 9, No. 12, 5097–5110, 2002.
17. Kral'kina, E. A., "Low-pressure radio-frequency inductive discharge and possibilities of optimizing inductive plasma sources," *Phys. Uspekhi*, Vol. 51, No. 5, 493–512, 2008.
18. Luk'yanchuk, B. and V. Ternovsky, "Light scattering by a thin wire with a surface-plasmon resonance: Bifurcations of the Poynting vector field," *Phys. Rev. B*, Vol. 73, No. 23, 235432, 2006.
19. Luk'yanchuk, B. S., M. I. Tribelsky, V. Ternovsky, Z. B. Wang, M. H. Hong, L. P. Shi, and T. C. Chong, "Peculiarities of light scattering by nanoparticles and nanowires near plasmon resonance frequencies in weakly dissipating materials," *J. Opt. A: Pure Appl. Opt.*, Vol. 9, No. 9, S294–S300, 2007.